ADVANCED FUNCTIONAL MATERIALS
www.afm-journal.de

Engineering of Push-Pull Thiophene Dyes to Enhance Light Absorption and Modulate Charge Recombination in Mesoscopic Solar Cells

Ning Cai, Yinglin Wang, Mingfei Xu, Ye Fan, Renzhi Li, Min Zhang,* and Peng Wang**

The elaborate selection of diverse π-conjugated segments which bridge the electron donors and acceptors in organic push-pull dyes can not only tune the molecular energy-levels but also impact the interfacial energetics and kinetics of dye-sensitized solar cells (DSCs). In this paper, a series of triphenylamine-cyanoacrylic acid photosensitizers is reported with TT, EDOT-BT, EDOT-CPDT, and CPDT-EDOT (herein TT, EDOT, BT, and CPDT denote terthiophene, ethylenedioxythiophene, bithiophene, and cyclopentadithiophene, respectively) as the π-linkers, and the dye-structure correlated photocurrent and photovoltage features of DSCs based on a cobalt electrolyte are scrutinized via analyzing light absorption and multichannel charge transfer kinetics. Both stepwise incorporation of more electron-rich blocks and rational modulation of connection order of dissimilar segments can result in a negative movement of ground-state redox potential and a red-shift of the absorption peak. While these styles of reducing energy-gap do not exert too much influence on the electron injection from photoexcited dye molecules to titania, the dyestuff employing the EDOT-BT linker presents a faster interfacial charge recombination and a slower dye regeneration, accounting for its inferior cell efficiency of 5.3% compared to that of 9.4% at the AM1.5G conditions achieved by the CPDT-EDOT dye.

1. Introduction

The search for viable tactics on transformation of inexhaustible sunlight into sustainable energy reserves such as clean electricity and solar fuels is presently one of the momentous global challenges. During the past two decades, a great amount of research passion has been caught on dye-sensitized solar cells (DSCs), a promising photovoltaic technology based on the use of low-cost materials and easy manufacturing processes.[1,2] In an efficient DSC, light absorption by dye molecules grafted on a mesoporous titania film is instantly followed by electron injection into titania. To achieve a good charge collection, photoinjected electrons in titania must traverse several micrometers to the current collector before being captured by electron acceptors. Consecutive material innovation has impelled the advancement of cell performance, and the highest reported power conversion efficiency has now reached 12.3% at the simulated AM 1.5G conditions.[3]

The development of metal-free organic dyes has been one of the recent research focuses, on primary account of their molecular tailoring flexibility and raw material abundance.[4,5] The design of capable organic push-pull dyes should at least consider two aspects of (i) reducing the molecular energy gap to absorb more solar photons and (ii) tuning the electronic as well as steric structures to regulate the energetics and kinetics at the titania/dye/electrolyte interface. The rational option of conjugated π-linkers is of paramount importance in the cell performance control, apart from electron donors and acceptors. In this respect, thiophene and its numerous derivatives have been actively exploited as the building blocks of organic chromophores[6–17] since their initial incorporation in the DSC coumarin dyes.[18] The various thiophene-based blocks furnish a flexible structural modification of photosensitizers, which on the other hand could bring forth complicated dye structure correlated photovoltaic behaviors.

In this contribution, we synthesize four thiophene dyes (**Figure 1**) with TT, EDOT-BT, EDOT-CPDT, and CPDT-EDOT (TT, EDOT, BT, and CPDT denote terthiophene, ethylenedioxythiophene, bithiophene, and cyclopentadithiophene, respectively) as the conjugated linkers in combination with the diethylhexyloxy-substituted triphenylamine donor and cyanoacrylic acid acceptor, to take a close look at the merit of utilizing more electron-rich conjugated segments in push-pull sensitizers to extend their spectral response to low energy solar photons. The dependence of important photovoltaic features such as external quantum efficiency and photovoltage on the energy level modulation, is detailed via measuring transient photophysical and electrical signals to examine multi-channel charge transfer kinetics.

N. Cai, Dr. Y. Wang, Dr. M. Xu, Y. Fan, Dr. R. Li,
Dr. M. Zhang, Prof. P. Wang
State Key Laboratory of Polymer Physics and Chemistry
Changchun Institute of Applied Chemistry
Chinese Academy of Sciences
Changchun, 130022, China
E-mail: renzhi.li@ciac.jl.cn; min.zhang@ciac.jl.cn; peng.wang@ciac.jl.cn

DOI: 10.1002/adfm.201202562

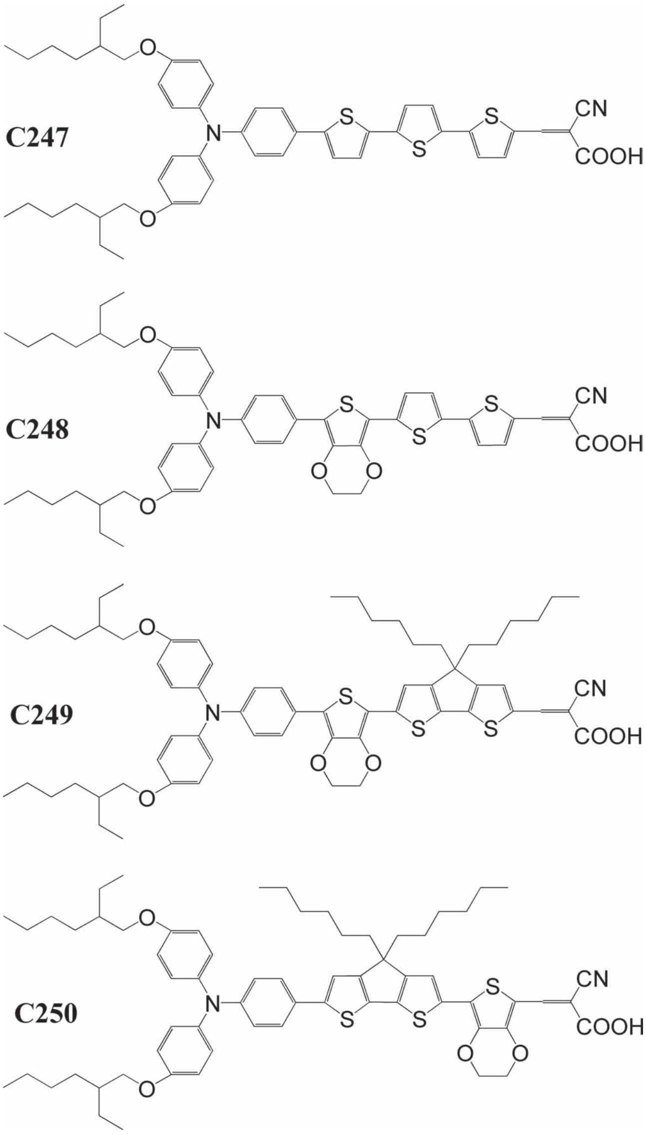

Figure 1. Structures of the triphenylamine-cyanoacrylic acid photosensitizers synthesized.

2. Results and Discussion

The light harvesting capacities of C247–C250 were first evaluated by recording their electronic absorption spectra (**Figure 2**) of diluted tetrahydrofuran (THF) solutions, and the detailed parameters were collected in **Table 1**. The maximum absorption wavelength ($\lambda_{\mathrm{max}}^{\mathrm{abs}}$) of the C247 model dye with the TT π-linker peaks at 485 nm, which is red-shifted to 522 nm upon replacing the thiophene unit adjacent to the triphenylamine donor with EDOT for C248. Further substituting the remaining two thiophene units (BT) with CPDT leads to a 34 nm red-shift of $\lambda_{\mathrm{max}}^{\mathrm{abs}}$ and a remarkably augmented maximum molar absorption coefficient ($\varepsilon_{\mathrm{max}}^{\mathrm{abs}}$) from 38×10^3 to 65×10^3 $\mathrm{M^{-1}\ cm^{-1}}$ with a comparison of C248 and C249. Interestingly, moving the CPDT moiety toward the triphenylamine side for C250 also red-shifts the $\lambda_{\mathrm{max}}^{\mathrm{abs}}$ from 556 to 563 nm. The calculated $S_0 \rightarrow S_1$ excitation energies ($E_{\mathrm{cal}}^{\mathrm{ex}}$) at the MPW1K/6-31G** level listed in Table 1 are in good agreement with the measured red-shifts of $\lambda_{\mathrm{max}}^{\mathrm{abs}}$ from C247 to C250. Further analyses on the molecular orbital topologies (Figure S1, Supporting Information) involving the $S_0 \rightarrow S_1$ transitions disclose that the low-energy absorption bands of C247–C250 are mainly assigned to the intramolecular charge transfer transitions from the triphenylamine donors and their adjacent conjugated units to cyanoacrylic acid acceptors and their adjoining segments.

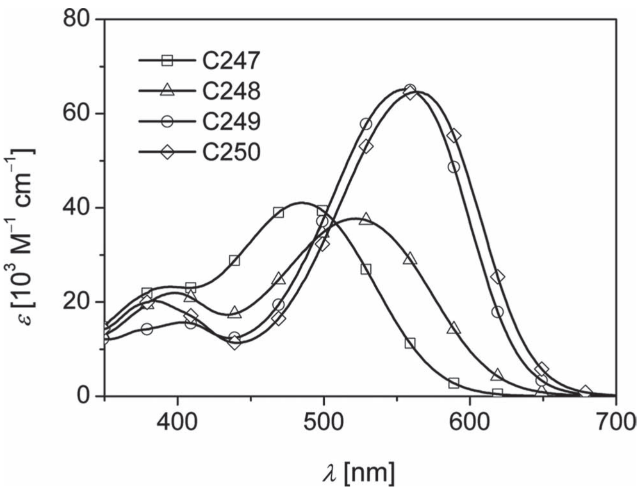

Figure 2. UV-vis absorption spectra of the triphenylamine-cyanoacrylic acid photosensitizers in THF.

Apart from the light absorption property of a sensitizer, the energy-offsets of dye molecules with respect to the titania nanocrystals and redox electrolytes also play a pivotal role in determining some subsequent dynamic processes such as exciton dissociation and long-range charge separation at the titania/dye/electrolyte interface, which may also have profound influences on the ultimate power output of a DSC. Thereby we derived the ground-state redox potentials ($E_{\mathrm{D/D^+}}$) of four dyes dissolved in THF through measuring square-wave voltammograms (**Figure 3**). As listed in Table 1, the values of $E_{\mathrm{D/D^+}}$ become low along with the use of more electron-rich units, being 0.22 V for C247, 0.14 V for C248, 0.11 V for C249, and 0.09 V for C250 against the standard ferrocene/ferrocenium (Fc/Fc$^+$) redox couple. On the basis of the zero-zero transition energies (E_{0-0}) estimated from the intersection points of normalized absorption and photoluminescence (PL) spectra (Figure S2, Supporting Information), we could calculate the exited state redox potential via the equation $E_{\mathrm{D^*/D^+}} = E_{\mathrm{D/D^+}} - E_{0-0}/\mathrm{e}$ without considering any entropy change during light excitation, being –1.95, –1.97, –1.85, and –1.86 V for C247, C248, C249, and C250, respectively.

The incident photon-to-collected electron conversion efficiencies (IPCEs) of these dyes were further tested in the mesoscopic titania solar cells based on a tris(2,2′-bipyridine)cobalt(II/III) electrolyte, the composition of which is described in the experimental section. As depicted in **Figure 4**, the onset wavelengths of photocurrent response are stepwise red-shifted from C247 to C250, which are in general accord with electronic absorptions of 2.3-µm-thick, dye-coated titania films immersed in the cobalt

Table 1. Photophysical and electrochemical data of C247, C248, C249, and C250 in THF.

Dye	$E_{\mathrm{cal}}^{\mathrm{ex}}$ [eV][a)]	$\lambda_{\mathrm{max}}^{\mathrm{abs}}$ [nm][b)]	$\varepsilon_{\mathrm{max}}^{\mathrm{abs}}$ [10^3 M^{-1} cm^{-1}][b)]	$\lambda_{\mathrm{max}}^{\mathrm{pl}}$ [nm][b)]	E_{0-0} [eV][c)]	$E_{\mathrm{D/D^+}}$ [V][d)]	$E_{\mathrm{D^*/D^+}}$ [V][e)]
C247	2.29	485	41	650	2.17	0.22	–1.95
C248	2.22	522	38	664	2.11	0.14	–1.97
C249	2.18	556	65	702	1.96	0.11	–1.85
C250	2.17	563	63	702	1.95	0.09	–1.86

[a)] The $S_0 \rightarrow S_1$ excitation energy ($E_{\mathrm{cal}}^{\mathrm{ex}}$) were calculated at the MPW1K/6-31G** level with the C-PCM model of THF; [b)] The maximum absorption wavelength (λ_{max}^{abs}), maximum molar absorption coefficient ($\varepsilon_{max}^{\mathrm{abs}}$), and PL maximum wavelength ($\lambda_{max}^{\mathrm{pl}}$) were derived from the static electronic absorption and emission spectra in THF solutions; [c)] The zero-zero transition energy (E_{0-0}) was estimated from the intersection point of normalized absorption and emission spectra; [d)] The ground-state redox potential ($E_{\mathrm{D/D^+}}$) is reported with Fc/Fc$^+$ as reference; [e)] The excited-state redox potential ($E_{\mathrm{D^*/D^+}}$) was estimated by equation $E_{\mathrm{D^*/D^+}} = E_{\mathrm{D/D^+}} + E_{0-0}/e$ without considering any entropy change during the light excitation.

electrolyte (Figure S3, Supporting Information). However, it is noteworthy that the C248 dye possesses a remarkably lower IPCE summit of 62% at 480 nm in contrast to the other three counterparts (79% at 490 nm for C247, 76% at 490 nm for C249, and 81% at 520 nm for C250), albeit the absorptances at the corresponding wavelengths of even transparent dye-coated titania films are all over 94%.

To understand the origins of IPCE maximum fluctuation, we utilized the time-correlated single photon counting technique to examine the possible impact of alternating $E_{\mathrm{D^*/D^+}}$ upon the yield of electron injection from excited-state dye molecules to titania.[19,20] Employing a C247, C248, C249, or C250-coated nanoporous alumina film infiltrated with the cobalt electrolyte, a dummy cell was assembled, which exhibited a strong red light emission upon exposing to 488 nm laser. On account of the lack of energy offset for electron injection at the interface between alumina and dye, the PL decays (dotted curves in **Figure 5**) could be ascribed to the radiative and nonradiative deactivation of excited-state dye molecules (D*). However, the substitution of alumina with titania brings on significant PL quenching, indicative of exciton dissociation at the energy-offset titania/dye interface (lines in Figure 5). By comparing the integral areas of PL traces of dye-coated titania and alumina films, we estimated the electron injection yields of the C247, C248, C249, and C250 cells, being 97%, 97%, 94%, and 94%, respectively. Thereby we conclude that the exciton dissociation yield is not the determinant factor controlling the IPCE summit, notwithstanding the presence of a similar but minor quantity of non-electron-injecting dye molecules in our cells.

We further carried out nanosecond transient absorption (TA) experiments to measure the kinetics of dual-channel charge-transfer reactions of oxidized dye molecules (D$^+$) with photo-injected electrons in the titania film and electron-donating species in the cobalt electrolyte, which may also affect the IPCE height. The oxidized states of C247–C250 all exhibit strong absorptions in the near-infrared region (**Figure 6**) in contrast to their neutral counterparts. Thereby in kinetic measurements we selected the probe light of 765 nm on the other account of the signal sensitivity of our photomultiplier tube detector,

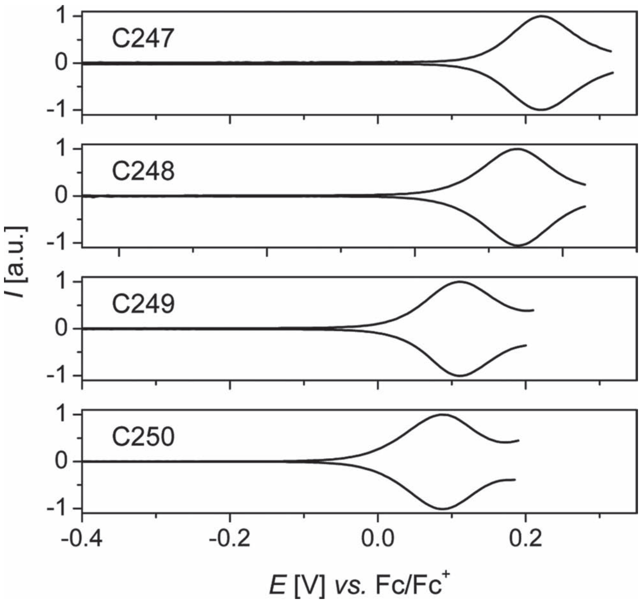

Figure 3. Square-wave voltammograms of dyes in THF with 0.1 M 1-ethyl-3-methylimidazolium bis(trifluoromethanesulfonyl)imide (EMITFSI) supporting electrolyte.

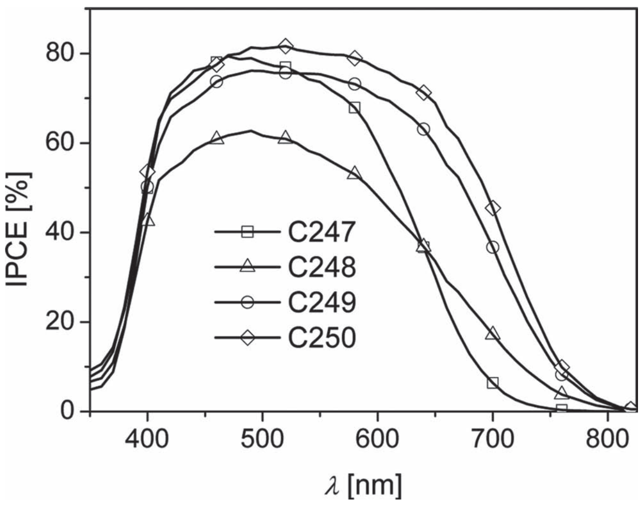

Figure 4. Photocurrent action spectra of the triphenylamine-cyanoacrylic acid dyes in the mesoscopic titania solar cells with a cobalt electrolyte.

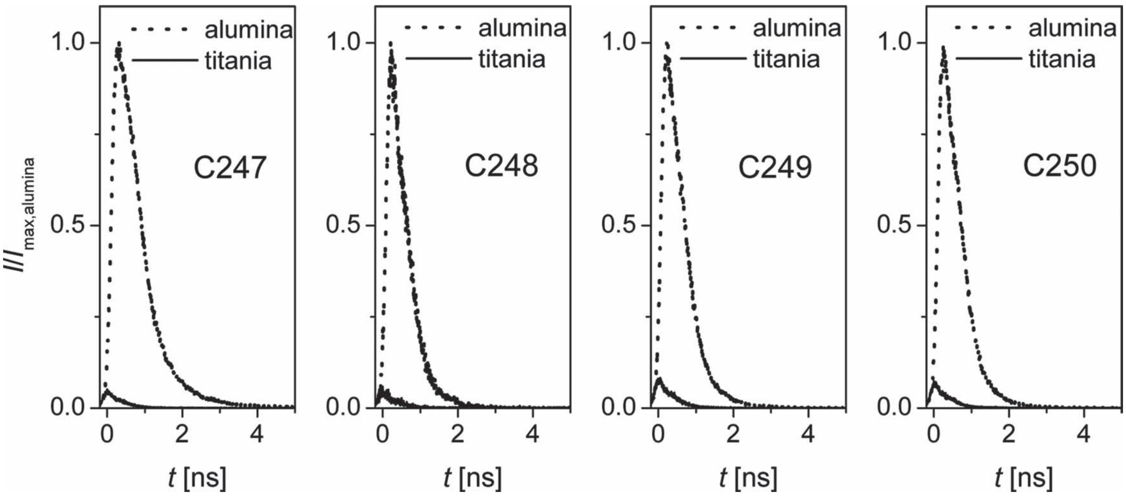

Figure 5. Time-resolved PL decay traces of dye-grafted mesoporous alumina (dotted curves) or titania film (lines) immersed in the cobalt electrolyte for cell fabrication. Excitation wavelength: 488 nm. The emission intensity (I) was corrected in term of the film absorbance at 488 nm and further normalized with the PL maximum of the dye-coated alumina film ($I_{\text{max, alumina}}$).

and also carefully chose the excitation wavelengths in terms of a ≈0.2 optical density of dye-coated titania films to ensure an alike exciton distribution profile in our testing cells. The rate of charge recombination between the photoinjected electrons in titania and oxidized dyes can be derived by recording the TA decays (traces a–d in **Figure 7**) of dummy cells, made from 11.0-µm-thick, dye-coated titania films soaked in the inert electrolyte composed of 0.5 M 4-*tert*-butylpyridine (TBP) and 0.1 M lithium bis(trifluoromethanesulfonyl)imide (LiTFSI) in acetonitrile (AN). The absorption traces can be fitted to a stretched exponential decay function $\Delta A \propto A_0 \exp[-(t/\tau)^{\alpha}]$, where A_0 is the pre-exponential factor, α is the stretching parameter, and τ is the characteristic time. Utilizing the gamma function $\Gamma(x)$, the mean times of these charge recombination reactions ($<\tau>_{\text{rec}}$) were derived through $<\tau> = (\tau/\alpha)\Gamma(1/\alpha)$[21] and compiled in Table S1 (Supporting Information). In general, substitution of the thiophene unit conjugated to triphenylamine with EDOT

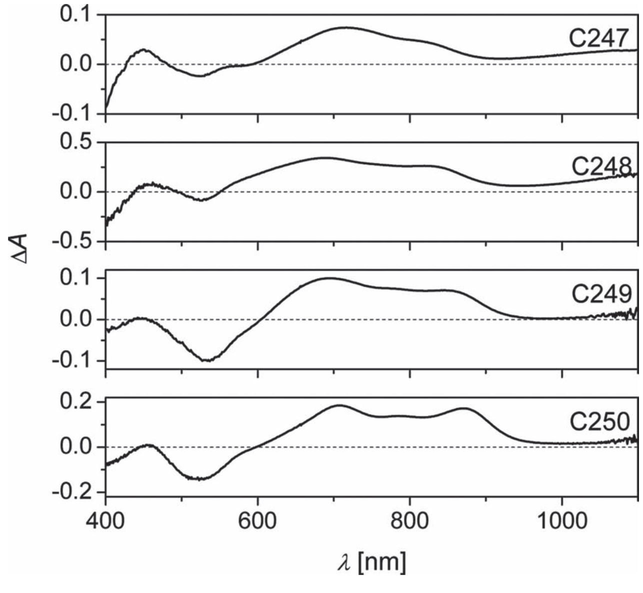

Figure 6. Absorption change as a function of wavelength upon applying a small positive potential to a 2.4-um-thick, dye-coated titania film dipped in EMITFSI.

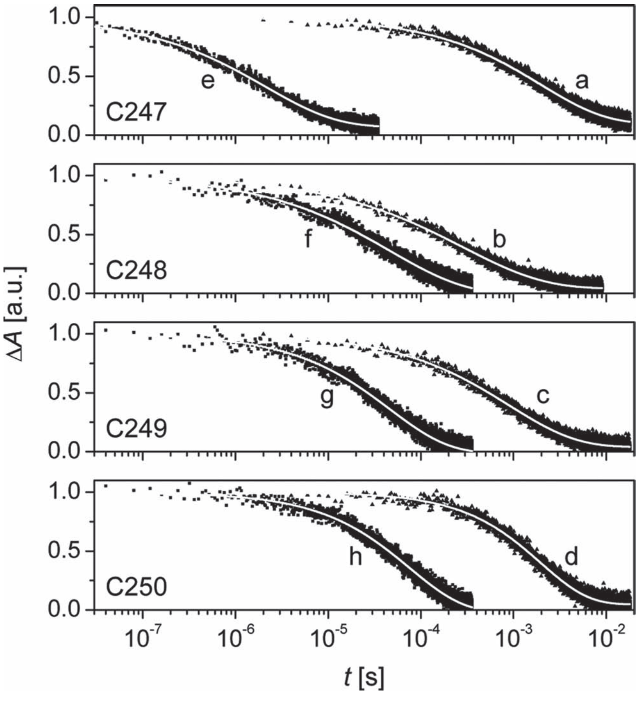

Figure 7. Transient absorption traces probed at 765 nm of 11.0-µm-thick, dye-coated titania films soaked with the inert (a–d) and cobalt (e–h) electrolytes. Laser pulse fluence and excitation wavelength: a) 18 µJ cm^{-2} at 655 nm; b) 17 µJ cm^{-2} at 719 nm; c) 16 µJ cm^{-2} at 733 nm; d) 16 µJ cm^{-2} at 727 nm; e) 18 µJ cm^{-2} at 661 nm; f) 16 µJ cm^{-2} at 730 nm; g) 16 µJ cm^{-2} at 741 nm; and h) 16 µJ cm^{-2} at 734 nm. Smooth lines are stretched exponential fittings over raw data obtained by averaging 700 laser shots.

brings forth evident accelerations of charge recombination, suggesting that there may be a hydrogen-bonding interaction of the ethylenedioxyl group with the active hydroxyls on the surface of titania, which will shorten the tunneling distance between electrons trapped in the titania nanocrystals and holes localized on the oxidized dye molecules.[22,23] The adverse interaction seems to be more or less attenuated via the introduction of two hydrophobic hexyl groups attached on CPDT in the cases of C249 and C250.

However, replacing the inert electrolyte with the cobalt electrolyte induced noticeably accelerated absorption decays (traces e–h in Figure 7), indicating the arising of rapid electron transfer from the tris(2,2′-bipyridine)cobalt(II) cations in the electrolyte to the oxidized dye molecules. Based on the same protocol presented above, the mean reaction times ($<\tau>_{\mathrm{reg}}$) of dye regeneration were also calculated and listed in Table S1 (Supporting Information). It is observed that the replacement of thiophene with electron-richer EDOT from C247 to C248 evidently slows down the dye regeneration rate, on probable account of a negative shift of $E_{\mathrm{D/D^+}}$ which reduces the absolute value of the Gibbs free energy for this charge transfer reaction. However, the positive correlation between $E_{\mathrm{D/D^+}}$ and dye regeneration rate is broken down along with the stepwise negative shift of $E_{\mathrm{D/D^+}}$ from C248 to C250 induced by the incorporation of electron-richer CPDT instead of BT as well as the modulation of the connection sequence of EDOT and CPDT. This finding may suggest the dominant roles of reorganization energy and electronic coupling factor[24] in the charge transfer reactions discussed here, both of which could be considerably affected by the microstructures of dye assemblies on titania. The speedy recombination and sluggish regeneration of C248 relative to other three dyes jointly lead to an evident decline of the long-range charge separation yield (φ_{lcs}) of 83%, compared to those of 100%, 95%, and 96% for C247, C249, and C250, respectively, explaining the aforementioned IPCE summits. It is noted that there is not a satisfactory linear correlation between the IPCE summit and φ_{lcs}, which could be ascribed to the influences of light absorption, charge collection yield, and the laser intensity dependent long-range charge separation yield.

The photocurrent density–voltage (*j*–*V*) characteristics (**Figure 8**A) of cells made from titania films coated by C247–C250 in conjunction with the cobalt electrolyte were recorded under the irradiance of 100 mW cm^{-2}, simulated AM1.5 sunlight and the detailed photovoltaic parameters were listed in **Table 2**. Among these four dyes, the C250 sensitizer presents the highest open-circuit photovoltage (V_{oc}) of 0.78 V and the largest short-circuit photocurrent density (j_{sc}) of 16.2 mA cm^{-2}, affording a power conversion efficiency of 9.4%. We also measured the current density–voltage (*j*–*V*) curves of these four cells at various light intensities and plotted V_{oc} as a function of j_{sc} in Figure 8B. Assuming that j_{sc} is proportional to photocarrier generation flux, we can compare the difference of V_{oc} at the same photocarrier generation flux. It is noted that at a given j_{sc}, the C250 dye possesses the highest photovoltage among these dyes whereas C248 presents the lowest one. The comparison on these two dyes is the focus of our further electrical analyses.

For a given redox electrolyte, we can ascribe the observed rise or fall of V_{oc} of DSCs to the shift of electron quasi-Fermi-level ($E_{\mathrm{F,n}}$) in titania, which could be associated with a movement of titania conduction band edge (E_{c}) and/or a variation of electron density.[25–28] At a certain flux of photocarrier generation, the electron density is dominated by the interfacial recombination of titania electrons with electron-accepting species in electrolytes and/or dye cations. Thus, we performed transient photovoltage decay and charge extraction experiments to understand the physical origin of V_{oc} variation. It is noted that there is ≈25 mV downward shift of the conduction-band edge of titania

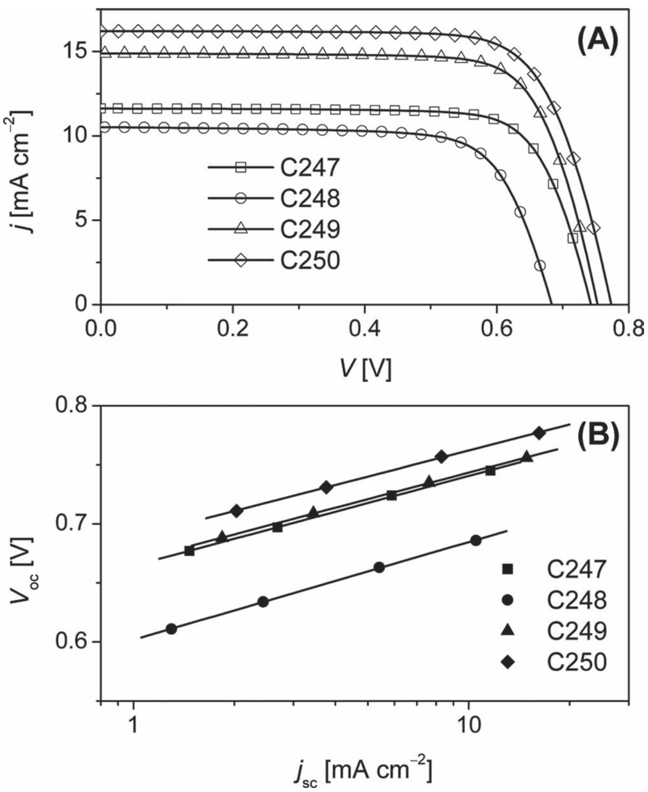

Figure 8. A) *j*–*V* characteristics measured under irradiation of 100 mW cm^{-2}, simulated AM1.5 sunlight. B) Plots of open-circuit photovoltage (V_{oc}) versus short-circuit photocurrent density (j_{sc}). An antireflection film was adhered to a testing cell during measurements. Aperture area of the employed metal mask: 0.158 cm^2.

Table 2. Photovoltaic parameters obtained at the simulated AM1.5G conditions.[a)]

Dye	j_{sc} [mA cm^{-2}]	V_{oc} [V]	FF	η [%]
C247	11.6	0.75	0.76	6.6
C248	10.5	0.69	0.73	5.3
C249	14.9	0.76	0.75	8.5
C250	16.2	0.78	0.74	9.4

[a)] The validity of our photovoltaic data is confirmed by comparing the calculated j_{sc} via wavelength integration of the product of the standard AM1.5 emission spectrum (ASTM G173-03) and measured IPCE spectra with the experimental j_{sc}, showing a less than 5% error. Also note that all our cells show a linear dependence of photocurrent on light intensity as shown in Figure S4 (Supporting Information).

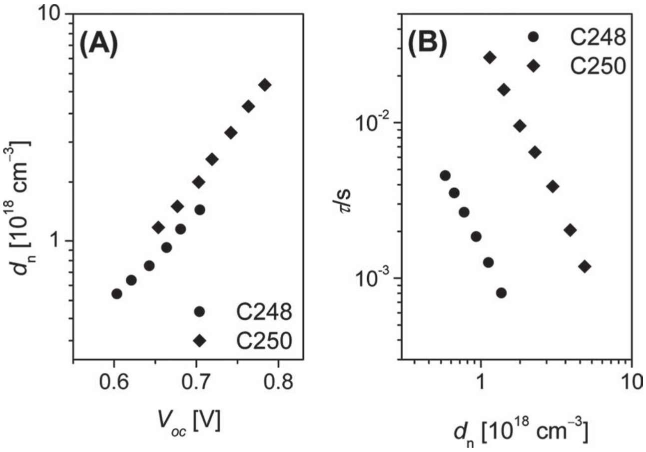

Figure 9. A) Extracted electron density in titania against open-circuit photovoltage and B) electron lifetime as a function of extracted electron density for cells made with titania films coated by C248 and C250.

when the sensitizer is changed from C248 to C250, which can be deduced from **Figure 9**A by comparing the extracted electron density (d_n) at the same potential bias. However, for the C250 cell there is an over one order of magnitude longer charge recombination lifetime (τ_n) at a given d_n (Figure 9B), which outreaches the adverse effect of a lower conduction-band edge, explaining its superior photovoltage at a given j_{sc} (Figure 8B). We also note that the charge recombination attenuation along with the sensitizer alternation form C248 to C250 is not caused by the dye load amount variation (C248, 2.4×10^{-8} mol cm^{-2} μm^{-1}; C250, 1.7×10^{-8} mol cm^{-2} μm^{-1}) but likely induced by the lateral molecular diameter augmentation.

3. Conclusions

We have synthesized four new organic sensitizers featuring stepwise shifts of both low-energy absorption peak and ground-state redox potential, and the C250 dye displays an excellent power conversion efficiency of 9.4% measured under the 100 mW cm^{-2}, simulated AM1.5 sunlight in conjunction with a tris(2,2′-bipyridine)cobalt(II/III) redox couple. The employment of electron-rich conjugated blocks has been demonstrated as a viable strategy to narrow down the energy gap of organic DSC dyes for efficient solar photon capture, without impacting the exciton dissociation efficiency at the titania/dye interface. We have also observed the breakdown of positive correlation between dye regeneration rate and ground-state redox potential of sensitizers, suggesting the vital role of the dye assembly microstructure on titania in charge transfer kinetics. This finding could be reasonably exploited in the future dye design, albeit the necessity for an appropriate energy-offset between dye and redox couple for swift dye regeneration. Our work has also shown that the dye-structure related interfacial charge recombination of titania electrons with electrolytes and/or oxidized dye molecules is one of the key determinant of cell photovoltage, which needs to be paid much attention in the development of new sensitizers.

4. Experimental Section

Materials: AN and THF were distilled before use and other reagents were purchased from commercial sources and used without further purification. 4,4,5,5-Tetramethyl-2-{4-[*N*,*N*-bis(4-(2-ethylhexyloxy)phenyl)amino]phenyl}-1,3,2-dioxaborolane,[29] 4-(3,4-ethylenedioxythiophene-5-yl)-*N*,*N*-bis(4-(2-ethylhexyloxy)phenyl)aniline,[30] 6-bromo-4,4-dihexyl-4*H*-cyclopenta[2,1-*b*:3,4-*b′*]dithiophene-2-carbaldehyde,[31] 6-{4-[*N*,*N*-bis(4-(2-ethylhexyloxy)phenyl)-amino]phenyl}-4,4-dihexyl-4*H*-cyclopenta[2,1-*b*:3,4-*b′*]dithiophene,[29] 5-bromo-5′′-formyl-2,2′:5′′,2′′-terthiophene,[32] 5′-bromo-2,2′-bithiophene-5-carbaldehyde,[33] and 5-bromo-3,4-ethylenedioxy-2-formylthiophene[34] were synthesized according to the corresponding literature methods. The Suzuki–Miyaura or Stille cross-coupling of bromine substituted aldehydes with a pinacol triaryl boronate or an aromatic stannane produced the dye precursors, which were further converted to the title cyanoacrylic acids by the classical Knoevenagel condensation reaction. The synthetic details are described as follows.

5-{4-[N,N-Bis(4-(2-ethylhexyloxy)phenyl)amino]phenyl}-2,2′:5′,2′′-terthiophene-5′′-carbaldehyde: To a stirred solution of 5-bromo-5′′-formyl-2,2′:5′,2′′-terthiophene (0.707 g, 1.991 mmol), 4,4,5,5-tetramethyl-2-{4-[*N*,*N*-bis(4-(2-ethylhexyloxy)phenyl)amino]phenyl}-1,3,2-dioxaborolane (1.500 g, 2.389 mmol), and K_3PO_4 (2.113 g, 9.955 mmol) in dioxane/H_2O (v/v, 5/1, 55 mL) was added 2-dicyclohexylphosphino-2′,6′-dimethoxybiphenyl (16 mg, 0.040 mmol) and palladium acetate (8 mg, 0.040 mmol). The reaction was carried out at 45 °C under argon for 5 h and then cooled to room temperature. The solution was extracted with ethyl acetate before the organic phase was washed with water and dried over anhydrous sodium sulfate. After evaporation of the solvent under reduced pressure, the crude product was purified by column chromatography over silica gel with dichloromethane/petroleum ether (v/v, 2/1) as the eluent to afford an orange solid as the desired product (1.392 g, 90% yield). ^{1}H NMR (400 MHz, DMSO-d_6, δ): 9.88 (s, 1H), 8.00 (d, *J* = 4.0 Hz, 1H), 7.58 (d, *J* = 3.6 Hz, 1H), 7.55 (d, *J* = 4.0 Hz, 1H), 7.48 (d, *J* = 8.8 Hz, 2H), 7.40 (d, *J* = 4.0 Hz, 1H), 7.36 (d, *J* = 4.0 Hz, 1H), 7.34 (d, *J* = 3.6 Hz, 1H), 7.04 (d, *J* = 8.8 Hz, 4H), 6.92 (d, *J* = 8.8 Hz, 4H), 6.77 (d, *J* = 8.8 Hz, 2H), 3.84 (d, *J* = 5.6 Hz, 4H), 1.67 (m, 2H), 1.44 (m, 8H), 1.31 (m, 8H), 0.89 (m, 12H). ^{13}C NMR (100 MHz, DMSO-d_6, δ): 183.74, 155.70, 148.37, 145.07, 143.81, 141.16, 139.45, 139.24, 138.32, 133.27, 133.00, 128.15, 126.98, 126.29, 126.22, 125.14, 124.92, 124.43, 123.18, 118.94, 115.55, 70.12, 38.72, 29.93, 28.44, 23.32, 22.50, 13.93, 10.92. MS (ESI) *m*/*z* calcd. for ($C_{47}H_{53}NO_3S_3$): 775.3. Found: 776.5 ([M+H]$^+$). Anal. calcd. for $C_{47}H_{53}NO_3S_3$: C, 72.73; H, 6.88; N, 1.80. Found: C, 72.61; H, 7.01; N, 1.77.

5′-(7-(4-(Bis(4-(2-ethylhexyloxy)phenyl)amino)phenyl)-2,3-dihydrothieno[3,4-b][1,4]dioxin-5-yl)-2,2′-bithiophene-5-carbaldehyde: To a stirred solution of 4-(3,4-ethylenedioxythiophene-5-yl)-*N*,*N*-bis(4-(2-ethylhexyloxy)phenyl)aniline (3.102 g, 4.832 mmol) in anhydrous THF (50 mL) was added dropwise *n*-butyllithium (1.6 M in hexane, 3.322 mL, 5.315 mmol) at −78 °C. The resulting mixture was stirred at −78 °C for 1 h before tributylstannyl chloride (1.697 mL, 6.282 mmol) was added in one portion. The cold bath was then removed and the solution was stirred at room temperature for 6 h. Water (50 mL) was added to quench the reaction and the solution was extracted with ethyl ether before the organic phase was washed with water and dried over anhydrous sodium sulfate. The solvent was evaporated under reduced pressure to afford a viscous yellow liquid, the main component of which was identified by ^{1}H NMR as 4-(2-tributylstannyl-3,4-ethylenedioxythiophene-5-yl)-*N*,*N*-bis(4-(2-ethylhexyloxy)phenyl)aniline with 70% yield and used for next reactions without further purification. To a stirred solution of 5′-bromo-2,2′-bithiophene-5-carbaldehyde (0.301 g, 1.103 mmol) and 4-(2-tributylstannyl-3,4-ethylenedioxythiophene-5-yl)-*N*,*N*-bis(4-(2-ethylhexyloxy)phenyl)aniline (1.078 g, 1.158 mmol) in toluene (15 mL) was added $Pd(PPh_3)_2Cl_2$ (0.077 g, 0.110 mmol). The resulting mixture was refluxed for 15 h and then cooled to room temperature. After evaporation of the solvent under reduced pressure, the crude product was purified by column chromatography over silica gel with ethyl acetate/

petroleum ether (v/v, 1/10) as the eluent to obtain a reddish orange solid as the desired product (0.644 g, 70% yield). ^{1}H NMR (400 MHz, DMSO-d_6, δ): 9.87 (s, 1H), 7.98 (d, *J* = 4.0 Hz, 1H), 7.56 (d, *J* = 4.0 Hz, 1H), 7.53 (d, *J* = 4.0 Hz, 1H), 7.49 (d, *J* = 8.8 Hz, 2H), 7.23 (d, *J* = 3.6 Hz, 1H), 7.01 (d, *J* = 8.8 Hz, 4H), 6.91 (d, *J* = 8.0 Hz, 4H), 6.80 (d, *J* = 9.2 Hz, 2H), 4.47 (s, 2H), 4.39 (s, 2H), 3.83 (d, *J* = 5.6 Hz, 4H), 1.67 (m, 2H), 1.35 (m, 16H), 0.90 (m, 12H). ^{13}C NMR (150 MHz, DMSO-d_6, δ): 182.63, 155.37, 147.22, 145.57, 145.43, 140.55, 139.50, 139.13, 138.96, 138.70, 137.22, 136.01, 133.21, 132.20, 126.35, 126.25, 123.49, 119.14, 115.39, 114.69, 107.83, 70.31, 64.81, 64.33, 38.57, 29.73, 28.15, 22.05, 21.50, 13.30, 10.54. MS (ESI) *m*/*z* calcd. for ($C_{49}H_{55}NO_5S_3$): 833.32. Found: 834.32 ([M+H]$^+$). Anal. calcd. for ($C_{49}H_{55}NO_5S_3$): C, 70.55; H, 6.65; N, 1.68. Found: C, 70.50; H, 6.74; N, 1.65.

6-{2-{4-[N,N-Bis(4-(2-ethylhexyloxy)phenyl)amino]phenyl}-3,4-(ethylenedioxy)thiophen-5-yl}-4,4-dihexyl-4H-cyclopenta[2,1-b:3,4-b′]dithiophene-2-carbaldehyde: To a stirred solution of 6-bromo-4,4-dihexyl-4*H*-cyclopenta[2,1-*b*:3,4-*b*′]dithiophene-2-carbaldehyde (0.500 g, 1.103 mmol) and 4-(2-tributylstannyl-3,4-ethylenedioxythiophene-5-yl)-*N*,*N*-bis(4-(2-ethylhexyloxy)phenyl)aniline (1.078 g, 1.158 mmol) in toluene (15 mL) was added Pd(PPh$_3$)$_2$Cl$_2$ (0.077 g, 0.110 mmol). The resulting mixture was refluxed for 15 h and then cooled to room temperature. After evaporation of the solvent under reduced pressure, the crude product was purified by column chromatography over silica gel with ethyl acetate/petroleum ether (v/v, 1/30) as the eluent to obtain a red solid as the desired product (0.825 g, 74% yield). ^{1}H NMR (400 MHz, DMSO-d_6, δ): 9.81 (s, 1H), 7.95 (s, 1H), 7.49 (d, *J* = 9.0 Hz, 2H), 7.25 (s, 1H), 7.02 (d, *J* = 9.0 Hz, 4H), 6.91 (d, *J* = 9.0 Hz, 4H), 6.80 (d, *J* = 9.0 Hz, 2H), 4.45 (s, 2H), 4.38 (s, 2H), 3.83 (d, *J* = 5.4 Hz, 4H), 1.88 (m, 4H), 1.67 (m, 2H), 1.40 (m, 8H), 1.30 (m, 8H), 1.12 (m, 12H), 0.89 (m, 16H), 0.77 (t, *J* = 6.4 Hz, 6H). ^{13}C NMR (150 MHz, DMSO-d_6, δ): 182.66, 162.28, 157.16, 155.37, 147.19, 146.17, 142.43, 139.50, 138.95, 138.69, 137.21, 132.88, 130.82, 126.35, 126.25, 123.49, 119.14, 116.32, 115.39, 114.72, 107.66, 70.32, 64.81, 64.33, 53.35, 38.58, 36.47, 30.52, 29.74, 28.48, 28.16, 23.64, 23.16, 22.06, 21.50, 13.41, 13.31, 10.55. MS (ESI) *m*/*z* calcd. for ($C_{62}H_{79}NO_5S_3$): 1013.5. Found: 1014.8 ([M+H]$^+$). Anal. calcd. for $C_{62}H_{79}NO_5S_3$: C, 73.40; H, 7.85; N, 1.38. Found: C, 73.31; H, 7.79; N, 1.35.

5-{6-{4-[N,N-Bis(4-(2-ethylhexyloxy)phenyl)amino]phenyl}-4,4-dihexyl-4H-cyclopenta[2,1-b:3,4-b′]dithiophene-2-yl}-3,4-ethylenedioxythiophen-2-carbaldehyde: To a stirred solution of 6-{4-[*N*,*N*-bis(4-(2-ethylhexyloxy)phenyl)-amino]phenyl}-4,4-dihexyl-4*H*-cyclopenta[2,1-*b*:3,4-*b*′]dithiophene (0.900 g, 1.063 mmol) in anhydrous THF (10 mL) was added dropwise *n*-butyllithium (1.6 M in hexane, 0.730 mL, 1.170 mmol) at −78 °C. The resulting mixture was stirred at −78 °C for 3 h before tributylstannyl chloride (0.375 mL, 1.382 mmol) was added in one portion. The cold bath was then removed and the solution was stirred at room temperature overnight. Water (10 mL) was added to quench the reaction and the solution was extracted with ethyl ether before the organic phase was washed with water and dried over anhydrous sodium sulfate. The solvent was evaporated under reduced pressure to afford a viscous yellow liquid, the main component of which was identified by ^{1}H NMR as 4-(2-tributylstannyl-4,4-dihexyl-4*H*-cyclopenta[2,1-*b*:3,4-*b*′]dithiophene-6-yl)-*N*,*N*-bis(4-(2-ethylhexyloxy)phenyl)aniline with 90% yield and used for next reactions without further purification. To a stirred solution of 5-bromo-3,4-ethylenedioxy-2-formylthiophene (0.204 g, 0.818 mmol) and 4-(2-tributylstannyl-4,4-dihexyl-4*H*-cyclopenta[2,1-*b*:3,4-*b*′]dithiophene-6-yl)-*N*,*N*-bis(4-(2-ethylhexyloxy)phenyl)aniline (1.085 g, 0.957 mmol) in toluene (10 mL) was added Pd(PPh$_3$)$_2$Cl$_2$ (0.058 g, 0.082 mmol). The resulting mixture was refluxed for 6 h and then cooled to room temperature. After evaporation of the solvent under reduced pressure, the crude product was purified by column chromatography over silica gel with ethyl acetate/petroleum ether (v/v, 1/5) as eluent to obtain a red solid as the desired product (0.763 g, 92% yield). ^{1}H NMR (600 MHz, DMSO-d_6, δ): 9.82 (s, 1H), 7.50 (s, 1H), 7.47 (d, *J* = 9.0 Hz, 2H), 7.38 (s, 1H), 7.01 (d, *J* = 9.0 Hz, 4H), 6.92 (d, *J* = 9.0 Hz, 4H), 6.78 (d, *J* = 9.0 Hz, 2H), 4.50 (s, 4H), 3.83 (d, *J* = 6.0 Hz, 4H), 1.89 (m, 4H), 1.68 (m, 2H), 1.40 (m, 8H), 1.29 (m, 8H), 0.91 (m, 12H), 0.89 (m, 16H), 0.76 (t, *J* = 7.2 Hz, 6H). ^{13}C NMR (150 MHz, DMSO-d_6, δ): 178.43, 160.24, 157.48, 155.51, 149.22, 147.85, 145.92, 139.64, 138.80, 136.49, 133.05, 132.33, 126.65, 126.05, 125.76, 122.77, 120.26, 119.57, 116.83, 115.51, 112.71, 70.13, 65.20, 64.81, 53.62, 38.71, 36.47, 30.93, 29.92, 28.88, 28.43, 23.64, 23.31, 22.48, 21.95, 13.91, 13.79, 10.91. MS (ESI) *m*/*z* calcd. for ($C_{62}H_{79}NO_5S_3$): 1013.5. Found: 1014.2 ([M+H]$^+$). Anal. calcd. for $C_{62}H_{79}NO_5S_3$: C, 73.40; H, 7.85; N, 1.38. Found: C, 73.27; H, 7.77; N, 1.34.

2-Cyano-3-{5-{4-[N,N-bis(4-(2-ethylhexyloxy)phenyl)amino]phenyl}-2,2′:5′,2″-terthienyl-5″-yl}acrylic Acid (***C247***): To a stirred solution of 5-{4-[*N*,*N*-bis(4-(2-ethylhexyloxy)phenyl)amino]phenyl}-2,2′:5′,2″-terthiophene-5″-carbaldehyde (1.290 g, 1.664 mmol) and 2-cyanoacetic acid (0.424 g, 4.992 mmol) in chloroform (50 mL) was added piperidine (0.990 g, 11.648 mmol). The resulting mixture was refluxed for 12 h and then cooled to room temperature before being acidified with 2 M hydrochloric acid aqueous solution. The solution was extracted with chloroform before the organic phase was washed with water and dried over anhydrous sodium sulfate. After evaporation of the solvent under reduced pressure, the crude product was purified by column chromatography over silica gel with methanol/chloroform (*v*/*v*, 1/50) as eluent to yield a purple powder (1.233 g, 88% yield). ^{1}H NMR (400 MHz, DMSO-d_6, δ): 13.68 (s, 1H), 8.35 (s, 1H), 7.88 (d, *J* = 4.0 Hz, 1H), 7.55 (d, *J* = 4.0 Hz, 2H), 7.48 (d, *J* = 8.8 Hz, 2H), 7.40 (d, *J* = 3.6 Hz, 1H), 7.36 (d, *J* = 4.0 Hz, 1H), 7.34 (d, *J* = 3.6 Hz, 1H), 7.04 (d, *J* = 8.8 Hz, 4H), 6.93 (d, *J* = 8.8 Hz, 4H), 6.77 (d, *J* = 8.8 Hz, 2H), 3.83 (d, *J* = 5.6 Hz, 4H), 1.68 (m, 2H), 1.44 (m, 8H), 1.21 (m, 8H), 0.89 (m, 12H). ^{13}C NMR (100 MHz, DMSO-d_6, δ): 163.71, 155.66, 148.33, 145.07, 144.42, 143.82, 140.53, 139.42, 138.33, 134.20, 133.19, 133.04, 127.92, 126.92, 126.27, 126.17, 124.98, 124.84, 124.43, 123.16, 118.94, 117.02, 115.50, 98.51, 70.10, 38.71, 29.92, 28.43, 23.31, 22.48, 13.90, 10.90. HR-MS (ESI) *m*/*z* calcd. for ($C_{50}H_{54}N_2O_4S_3$): 842.32457. Found: 865.31314 ([M+Na]$^+$). Anal. calcd. for $C_{50}H_{54}N_2O_4S_3$: C, 71.22; H, 6.46; N, 3.32. Found: C, 71.14; H, 6.55; N, 3.28. IR (KBr): 1686 cm^{-1} (COOH), 2217^{-1} cm (CN).

2-Cyano-3-{5′-{2-{4-[N,N-bis(4-(2-ethylhexyloxy)phenyl)amino]phenyl}-3,4-(ethylenedioxy)thiophen-5-yl}-2,2′- bithienyl-5-yl}acrylic Acid (***C248***): To a stirred solution of 5′-(7-(4-(bis(4-(2-ethylhexyloxy)phenyl)amino)phenyl)-2,3-dihydrothieno[3,4-b][1,4]dioxin-5-yl)-2,2′-bithiophene-5-carbaldehyde (0.580 g, 0.695 mmol) and 2-cyanoacetic acid (0.177 g, 2.086 mmol) in chloroform (21 mL) was added piperidine (0.413 g, 4.865 mmol). The resulting mixture was refluxed for 12 h and then cooled to room temperature before being acidified with 2 M hydrochloric acid aqueous solution. The solution was extracted with chloroform before the organic phase was washed with water and dried over anhydrous sodium sulfate. After evaporation of the solvent under reduced pressure, the crude product was purified by column chromatography over silica gel with methanol/chloroform (v/v, 1/50) as eluent to yield a purple-black powder (0.551 g, 88% yield). ^{1}H NMR (600 MHz, DMSO-d_6, δ): 13.64 (s, 1H), 8.46 (s, 1H), 7.96 (d, *J* = 3.6 Hz, 1H), 7.57 (m, 2H), 7.48 (d, *J* = 8.4 Hz, 2H), 7.23 (d, *J* = 3.6 Hz, 1H), 7.01 (d, *J* = 8.4 Hz, 4H), 6.91 (d, *J* = 9.0 Hz, 4H), 6.78 (d, *J* = 8.4 Hz, 2H), 4.47 (s, 2H), 4.37 (s, 2H), 3.82 (d, *J* = 5.4 Hz, 4H), 1.65 (m, 2H), 1.36 (m, 16H), 0.89 (m, 12H). ^{13}C NMR (150 MHz, DMSO-d_6, δ): 163.13, 155.38, 147.27, 145.60, 145.46, 140.59, 139.46, 139.16, 137.14, 136.03, 133.24, 132.14, 127.04, 126.33, 124.15, 123.33, 123.24, 119.06, 116.08, 115.37, 106.53, 97.50, 70.34, 64.85, 64.28, 38.58, 29.72, 28.14, 23.15, 22.03, 13.38, 10.53. HR-MS (ESI) *m*/*z* calcd. for ($C_{52}H_{56}N_2O_6S_3$): 900.33005. Found: 923.31867 ([M+Na]$^+$). Anal. calcd. for ($C_{52}H_{56}N_2O_6S_3$): C, 69.30; H, 6.26; N, 3.11. Found: C, 69.21; H, 6.30; N, 3.09. IR (KBr): 1686 cm^{-1} (COOH), 2217 cm^{-1} (CN).

2-Cyano-3-{6-{2-{4-[N,N-bis(4-(2-ethylhexyloxy)phenyl)amino]phenyl}-3,4-(ethylenedioxy)thiophen-5-yl}-4,4-dihexyl-4H-cyclopenta[2,1-b:3,4-b′]dithiophene-2-yl}Acrylic Acid (***C249***): To a stirred solution of 6-{2-{4-[*N*,*N*-bis(4-(2-ethylhexyloxy)phenyl)amino]phenyl}-3,4-(ethylenedioxy)thiophen-5-yl}-4,4-dihexyl-4*H*-cyclopenta[2,1-*b*:3,4-*b*′]dithiophene-2-carbaldehyde (0.271 g, 0.270 mmol) and 2-cyanoacetic acid (0.068 g, 0.810 mmol) in chloroform (15 mL) was added piperidine (0.160 g, 1.880 mmol). The resulting mixture was refluxed for 12 h and then cooled to room temperature before being acidified with 2 M hydrochloric acid aqueous solution. The solution was extracted with chloroform before the organic phase was washed with water and dried over anhydrous sodium sulfate. After evaporation of the solvent under reduced pressure, the crude product was purified by column chromatography over silica gel with methanol/chloroform (v/v, 1/50) as eluent to yield a black powder (0.255 g, 89% yield) ^{1}H NMR (400 MHz, DMSO-d_6, δ): 13.35 (s, 1H), 8.40 (s, 1H), 7.91 (s, 1H), 7.50 (d, J = 8.8 Hz, 2H), 7.27 (s, 1H), 7.01 (d, J = 8.8 Hz, 4H), 6.91 (d, J = 8.8 Hz, 4H), 6.79 (d, J = 8.8 Hz, 2H), 4.45 (s, 2H), 4.38 (s, 2H), 3.83 (d, J = 5.6 Hz, 4H), 1.90 (m, 4H), 1.67 (m, 2H), 1.40 (m, 8H), 1.30 (m, 8H), 1.12 (m, 12H), 0.89 (m, 16H), 0.77 (t, J = 6.4 Hz, 6H). ^{13}C NMR (150 MHz, DMSO-d_6, δ): 163.79, 163.05, 157.26, 155.40, 148.32, 147.25, 146.45, 140.13, 139.47, 138.98, 137.24, 135.29, 133.04, 132.23, 126.38, 126.27, 123.42, 119.09, 116.91, 116.30, 115.39, 115.15, 107.71, 93.35, 70.33, 64.86, 64.33, 53.16, 38.59, 37.21, 30.51, 29.74, 28.46, 28.17, 23.17, 23.65, 22.07, 21.50, 13.42, 13.31, 10.56. HR-MS (ESI) m/z calcd. for ($C_{65}H_{80}N_2O_6S_3$): 1080.51785. Found: 1080.51246 ($[M]^+$). Anal. calcd. for $C_{65}H_{80}N_2O_6S_3$: C, 72.18; H, 7.46; N, 2.59. Found: C, 72.09; H, 7.54; N, 2.51. IR (KBr): 1678 cm^{-1} (COOH), 2210 cm^{-1} (CN).

2-Cyano-3-{5-{6-{4-[N,N-bis(4-(2-ethylhexyloxy)phenyl)amino]phenyl}-4,4-dihexyl-4H-cyclopenta[2,1-b:3,4-b′]dithiophene-2-yl}-3,4-ethylenedioxythiophen-2-yl}acrylic acid (***C250***): To a stirred solution of 5-{6-{4-[*N*,*N*-bis(4-(2-ethylhexyloxy)phenyl)amino]phenyl}-4,4-dihexyl-4*H*-cyclopenta[2,1-*b*:3,4-*b*′]dithiophene-2-yl}-3,4-ethylenedioxythiophen-2-carbaldehyde (0.530 g, 0.521 mmol) and 2-cyanoacetic acid (0.133 g, 1.564 mmol) in chloroform (20 mL) was added piperidine (0.310 g, 3.647 mmol). The resulting mixture was refluxed for 12 h and then cooled to room temperature before being acidified with 2 M hydrochloric acid aqueous solution. The solution was extracted with chloroform before the organic phase was washed with water and dried over anhydrous sodium sulfate. After evaporation of the solvent under reduced pressure, the crude product was purified by column chromatography over silica gel with methanol/chloroform (v/v, 1/50) as eluent to yield a black powder (0.503 g, 89% yield) ^{1}H NMR (600 MHz, THF-d_8, δ): 8.46 (s, 1H), 7.62 (m, 3H), 7.42 (s, 1H), 7.19 (d, J = 9.0 Hz, 4H), 7.06 (d, J = 9.0 Hz, 2H), 7.03 (d, J = 9.0 Hz, 4H), 4.64 (s, 4H), 4.03 (d, J = 5.4 Hz, 4H), 2.13 (m, 4H), 1.89 (m, 2H), 1.65 (m, 8H), 1.53 (m, 8H), 1.34 (m, 12H), 1.11 (m, 16H), 0.97 (t, J = 5.4 Hz, 6H). ^{13}C NMR (150 MHz, THF-d_8, δ): 165.27, 161.90, 159.14, 157.50, 149.90, 148.48, 142.50, 141.93, 140.91, 137.87, 135.39, 134.48, 128.48, 127.88, 127.14, 125.47, 121.87, 121.40, 117.98, 117.77, 116.52, 109.93, 94.67, 71.65, 67.34, 66.59, 55.59, 41.13, 39.37, 33.05, 32.05, 31.13, 30.56, 26.08, 25.30, 24.44, 23.99, 14.91, 14.85, 12.00. HR-MS (ESI) m/z calcd. for ($C_{65}H_{80}N_2O_6S_3$): 1080.51785. Found: 1080.51554 ($[M]^+$). Anal. calcd. for $C_{65}H_{80}N_2O_6S_3$: C, 72.18; H, 7.46; N, 2.59. Found: C, 72.06; H, 7.52; N, 2.49. IR (KBr): 1675 cm^{-1} (COOH), 2210 cm^{-1} (CN).

UV-Vis Absorption and Photoluminescence (PL) Measurements: Steady UV-vis absorption and PL spectra were measured with an Agilent G1103A spectrometer and a PerkinElmer LS55 luminescence spectrometer, respectively. The emitted light was tested with a Hamamatsu R928 red-sensitive photomultiplier. Transient absorption decay traces were recorded with a LP920 laser flash spectrometer with a tunable OPOLett 355II laser to supply the nanosecond excitation pulse. The PL decays were measured with a LifeSpec-II fluorescence spectrometer equipped with an EPL488 laser diode.

Computational Details: The ground state geometries were optimized employing the hybrid B3LYP[35] function and a 6-31G** basis set. Vertical excitation energies were calculated by TD-DFT at the MPW1K[36–38]/6-31G** levels. The effect of THF on the geometries and absorption spectra has been simulated by the C-PCM method.[39] All calculations were carried out with the Gaussian 09 program package.[40]

Redox Potential Measurements: Square-wave voltammograms of these four new dyes dissolved in THF were recorded on an Autolab-PGSTAT302N electrochemical workstation by use of a three-electrode electrolytic cell, consisting of a platinum gauze counter electrode, a silver wire auxiliary electrode, and a platinum ultramicroelectrode. All potentials were reported relative to the Fc/Fc$^+$ reference.

Cell Fabrication and Photovoltaic Characterization: A double layer titania film made via screen-printing on a precleaned fluorine-doped tin oxide (FTO) conducting glass (Nippon Sheet Glass, Solar, 4 mm thick) was deployed as the negative electrode of DSCs presented in this paper. A 2.3-µm-thick translucent layer of 25 nm sized titania particles was first deposited on a FTO glass and further covered with a 4.5-µm-thick light-scattering layer of 350–450 nm sized titania particles (WER4-O, Dyesol). Preparation procedures of titania nanocrystals, screen-printing pastes, and nanostructured titania films were very similar to those described in a previous paper.[41] A circular titania electrode (≈0.28 cm^2) was dye-loaded by immersing it into a 100 µM dye solution in the mixed solvent of AN and THF. The dye-coated titania electrode was assembled with a thermally platinized FTO electrode by use of a 25-µm-thick Surlyn ring to produce a thin-layer electrochemical cell. The infiltrated electrolyte is composed of 0.25 M tris(2,2′-bipyridine)cobalt(II) di[bis(trifluoromethanesulfonyl)-imide], 0.05 M tris(2,2′-bipyridine)cobalt(III) tris[bis(trifluoromethanesulfonyl)imide], 0.5 M TBP, and 0.1 M LiTFSI in AN. Details on photovoltaic characterizations can be found in our previous publication.[42]

Charge Extraction and Transient Photovoltage Decay Measurements: Transient photoelectrical experiments[43] were performed on an Autolab-PGSTAT302N electrochemical workstation with the ADC10M high-speed module, which can satisfy 100-ns time-resolved current and voltage tests. The static and perturbing lights were supplied with home-made white and red light-emitting diode arrays. We employed a red light to generate a photovoltage perturbation near the open-circuit photovoltage of a testing cell under the irradiation of a certain white light and measured the voltage decay thereafter. The modulated photovoltage by the red pulse of a testing cell is below 5 mV and the transient signals follow a mono-exponential decay. Fitting an exponential function to the photovoltage decay can produce the electron lifetime. The electron density was estimated by the charge extraction method. We first maintained a testing cell at open circuit under a white light and then changed it to short circuit upon switching off the light to record the concomitant current transients. Further calculation with integral of the current trace can generate the electron density.

Supporting Information

Supporting Information is available from the Wiley Online Library or from the author.

Acknowledgements

N.C., Y.W., and M.X. contributed equally to this work. The National Science Foundation of China (Nos. 50973105, 51125015, 51103146, and 21203175), the National 973 Program (No. 2011CBA00702), the National 863 Program (No. 2011AA050521), and the Key Scientific and Technological Program of Jilin Province (No. 10ZDGG012) are acknowledged for financial support. We are grateful to Dyesol for supplying the WER4-O scattering paste and to DuPont Packaging and Industrial Polymers for supplying the Surlyn and Bynel films.

Received: September 6, 2012

---

[1] B. O'Regan, M. Grätzel, *Nature* **1991**, *353*, 737.
[2] M. Grätzel, *Acc. Chem. Res.* **2009**, *42*, 1788.
[3] A. Yella, H.-W. Lee, H. N. Tsao, C. Yi, A. K. Chandiran, M. K. Nazeeruddin, E. W.-G. Diau, C. Y. Yeh, S. M. Zakeeruddin, M. Grätzel, *Science* **2011**, *334*, 629.
[4] A. Mishra, M. K. R. Fischer, P. Bäuerle, *Angew. Chem. Int. Ed.* **2009**, *48*, 2474.
[5] J. N. Clifford, E. Martínez-Ferrero, A. Viterisi, E. Palomares, *Chem. Soc. Rev.* **2011**, *40*, 1635.
[6] D. P. Hagberg, T. Edvinsson, T. Marinado, G. Boschloo, A. Hagfeldt, L. Sun, *Chem. Commun.* **2006**, 2245.

[7] N. Koumura, Z.-S. Wang, S. Mori, M. Miyashita, E. Suzuki, K. Hara, *J. Am. Chem. Soc.* **2006**, *128*, 14256.

[8] S. Kim, J. K. Lee, S. O. Kang, J. Ko, J.-H. Yum, S. Fantacci, F. De Anglis, D. Di Censo, M. K. Nazeeruddin, M. Grätzel, *J. Am. Chem. Soc.* **2006**, *128*, 16701.

[9] Z.-S. Wang, Y. Cui, K. Hara, Y. Dan-oh, C. Kasada, A. Shinpo, *Adv. Mater.* **2007**, *19*, 1138.

[10] K. R. J. Thomas, Y.-C. Lin, K.-M. Lee, K.-C. Ho, C.-H. Lai, Y.-M. Chen, P.-T. Chou, *Chem. Mater.* **2008**, *20*, 1830.

[11] H. Qin, S. Wenger, M. Xu, F. Gao, X. Jing, P. Wang, S. M. Zakeeruddin, M. Grätzel, *J. Am. Chem. Soc.* **2008**, *130*, 9202.

[12] D.-Y. Chen, Y.-Y. Hsu, H.-C. Hsu, B.-S. Chen, Y.-T. Lee, H. Fu, M.-W. Chung, S.-H. Liu, H.-C. Chen, Y. Chi, P.-T. Chou, *Chem. Commun.* **2010**, *46*, 5256.

[13] Y. Bai, J. Zhang, D. Zhou, Y. Wang, M. Zhang, P. Wang, *J. Am. Chem. Soc.* **2011**, *133*, 11442.

[14] Y. Cui, Y. Wu, X. Lu, X. Zhang, G. Zhou, F. B. Miapeh, W. Zhu, Z.-S. Wang, *Chem. Mater.* **2011**, *23*, 4394.

[15] M. Xu, M. Zhang, M. Pastore, R. Li, F. De Angelis, P. Wang, *Chem. Sci.* **2012**, *3*, 976.

[16] Y.-C. Chen, H.-H. Chou, M. C. Tsai, S.-Y. Chen, J. T. Lin, C.-F. Yao, K. Chen, *Chem. Eur. J.* **2012**, *18*, 5430.

[17] S. Haid, M. Marszalek, A. Mishra, M. Wielopolski, J. Teuscher, J.-E. Moser, R. Humphry-Baker, S. M. Zakeeruddin, M. Grätzel, P. Bäuerle, *Adv. Funct. Mater.* **2012**, *22*, 1291.

[18] K. Hara, M. Kurashige, Y. Dan-oh, C. Kasada, A. Shinpo, S. Suga, K. Sayama, H. Arakawa, *New J. Chem.* **2003**, *27*, 783.

[19] S. E. Koops, P. R. F. Barnes, B. O'Regan, J. R. Durrant, *J. Phys. Chem. C* **2010**, *114*, 8054.

[20] T. D. Santos, A. Morandeira, S. Koops, A. J. Mozer, G. Tsekouras, Y. Dong, P. Wagner, G. Wallace, J. C. Earles, K. C. Gordon, D. Officer, J. R. Durrant, *J. Phys. Chem. C* **2010**, *114*, 3276.

[21] A. Y. Anderson, P. R. F. Barnes, J. R. Durrant, B. O'Regan, *J. Phys. Chem. C* **2011**, *115*, 2439.

[22] H. Imahori, S. Kang, H. Hayashi, M. Haruta, H. Kurata, S. Isoda, S. E. Canton, Y. Infahsaeng, A. Kathiravan, T. Pascher, P. Chábera, A. P. Yartsev, V. Sundström, *J. Phys. Chem. A* **2011**, *115*, 3679.

[23] S. Mathew, H. Iijima, Y. Toude, T. Umeyama, Y. Matano, S. Ito, N. V. Tkachenko, H. Lemmetyinen, H. Imahori, *J. Phys. Chem. C* **2011**, *115*, 14415.

[24] R. A. Marcus, *J. Chem. Phys.* **1965**, *43*, 679.

[25] B. O'Regan, J. R. Durrant, *Acc. Chem. Res.* **2009**, *42*, 1799.

[26] F. Fabregat-Santiago, G. Garcia-Belmonte, I. Mora-Séro, J. Bisquert, *Phys. Chem. Chem. Phys.* **2011**, *13*, 9083.

[27] J. N. Clifford, E. Martínez-Ferrero, E. Polomares, *J. Mater. Chem.* **2012**, *22*, 12415.

[28] T. Stergiopoulos, P. Falaras, *Adv. Energy Mater.* **2012**, *2*, 616.

[29] J. Liu, D. Zhou, F. Wang, F. Fabregat-Santiago, S. G. Miralles, X. Jing, J. Bisquert, P. Wang, *J. Phys. Chem. C* **2011**, *115*, 14425.

[30] W. Zeng, Y. Cao, Y. Bai, Y. Wang, Y. Shi, M. Zhang, F. Wang, C. Pan, P. Wang, *Chem. Mater.* **2010**, *22*, 1915.

[31] R. Li, J. Liu, N. Cai, M. Zhang, P. Wang, *J. Phys. Chem. B* **2010**, *114*, 4461.

[32] T. Nishizawa, K. Tajima, K. Hashimoto, *J. Mater. Chem.* **2007**, *17*, 2440.

[33] S. P. G. Costa, R. M. F. Batista, M. M. M. Raposo, *Tetrahedron* **2008**, *64*, 9733.

[34] M. Jessing, M. Brandt, K. J. Jensen, J. B. Christensen, U. Boas, *J. Org. Chem.* **2006**, *71*, 6734.

[35] A. D. Becke, *J. Chem. Phys.* **1993**, *98*, 1372.

[36] B. J. Lynch, P. L. Fast, M. Harris, D. G. Truhlar, *J. Phys. Chem. A* **2000**, *104*, 4811.

[37] M. Cossi, V. Barone, *J. Chem. Phys.* **2001**, *115*, 4708.

[38] M. Pastore, E. Mosconi, F. De Angelis, M. Grätzel, *J. Phys. Chem. C* **2010**, *114*, 7205.

[39] M. Cossi, N. Rega, G. Scalmani, V. Barone, *J. Comput. Chem.* **2003**, *24*, 669.

[40] M. J. Frisch, G. W. Trucks, H. B. Schlegel, G. E. Scuseria, M. A. Robb, J. R. Cheeseman, G. Scalmani, V. Barone, B. Mennucci, G. A. Petersson, H. Nakatsuji, M. Caricato, X. Li, H. P. Hratchian, A. F. Izmaylov, J. Bloino, G. Zheng, J. L. Sonnenberg, M. Hada, M. Ehara, K. Toyota, R. Fukuda, J. Hasegawa, M. Ishida, T. Nakajima, Y. Honda, O. Kitao, H. Nakai, T. Vreven, J. A. Montgomery, J. E. Peralta, F. Ogliaro, M. Bearpark, J. J. Heyd, E. Brothers, K. N. Kudin, V. N. Staroverov, R. Kobayashi, J. Normand, K. Raghavachari, A. Rendell, J. C. Burant, S. S. Iyengar, J. Tomasi, M. Cossi, N. Rega, N. J. Millam, M. Klene, J. E. Knox, J. B. Cross, V. Bakken, C. Adamo, J. Jaramillo, R. Gomperts, R. E. Stratmann, O. Yazyev, A. J. Austin, R. Cammi, C. Pomelli, J. W. Ochterski, R. L. Martin, K. Morokuma, V. G. Zakrzewski, G. A. Voth, P. Salvador, J. J. Dannenberg, S. Dapprich, A. D. Daniels, Ö. Farkas, J. B. Foresman, J. V. Ortiz, J. Cioslowski, D. J. Fox, *Gaussian 09*, Revision A.1, Gaussian, Inc., Wallingford, CT **2009**.

[41] P. Wang, S. M. Zakeeruddin, P. Comte, R. Charvet, R. Humphry-Baker, M. Grätzel, *J. Phys. Chem. B* **2003**, *107*, 14336.

[42] J. Liu, R. Li, X. Si, D. Zhou, Y. Shi, Y. Wang, X. Jing, P. Wang, *Energy Environ. Sci.* **2010**, *3*, 1924.

[43] B. C. O'Regan, K. Bakker, J. Kroeze, H. Smit, P. Sommeling, J. R. Durrant, *J. Phys. Chem. B* **2006**, *110*, 17155.